Marine Structures 42 (2015) 115–136

Contents lists available at ScienceDirect

Marine Structures

journal homepage: www.elsevier.com/locate/marstruc

Corrosion fatigue load frequency sensitivity analysis

O. Adedipe*, F. Brennan, A. Kolios

Cranfield University, Bedfordshire MK43 0AL, United Kingdom

ARTICLE INFO

Article history:
Received 9 May 2014
Received in revised form 17 March 2015
Accepted 17 March 2015
Available online

Keywords:
Monopile
Offshore wind turbines
Seawater
Fatigue
Crack

ABSTRACT

This paper presents experimental assessment of crack growth rates of S355J2+N steel in a corrosion fatigue environment similar to what is experienced on offshore wind farm monopile structures under various cyclic load frequencies in order to assess the effect of cyclic frequency of the applied loading within a frequency range pertinent to the structure. Fatigue crack propagation behaviour in this test programme is evaluated through fatigue tests on six compact tension test specimens in air and in laboratory simulated seawater under free corrosion condition. Fatigue crack lengths were monitored by back face strain (BFS), DCPD and ACPD. A regression model was derived through the BFS method to express strain values as a function of crack length to width ratio. The effectiveness of BFS method is particularly demonstrated in the simulated marine environment. Within the range of test frequencies, crack growth rates in simulated seawater when compared to the equivalent air test revealed environmental reduction factors of 2 and 4 at lower and higher values of stress intensity factors respectively. Significant difference in the results of the seawater test frequencies is discussed.

1. Introduction

Corrosion and fatigue have been a dominant degradation mechanism for steel structures, with the combination of the two, known as corrosion fatigue having amplified effects in structures in the harsh

* Corresponding author.
E-mail address: o.adedipe@cranfield.ac.uk (O. Adedipe).

http://dx.doi.org/10.1016/j.marstruc.2015.03.005
0951-8339/

marine environments. Fatigue loads in typical offshore wind turbine support structures are mainly caused by wave, wind and operational loads from the rotor during operation. Therefore, offshore wind turbine monopile structures in deep waters have to be designed against corrosion fatigue in order to ensure their fitness for purpose. Corrosion is a time dependent mechanism and therefore corrosion fatigue tests need to be conducted at cyclic load frequencies representative of those experienced in service. However, understanding of dominant cyclic frequency is important when designing offshore wind turbines against corrosion fatigue. Lower cyclic frequencies are known to be more damaging under corrosion fatigue conditions for a number of reasons but mainly due to the longer time exposed to electrochemical corrosion elements per cycle. Also, cyclic frequency has a significant effect on the corrosion fatigue crack growth rates and therefore, a comprehensive understanding of the response of offshore wind farm monopile structures to dominant frequency is very important in order to produce realistic outcomes in laboratory test programmes similar to what is experienced in service.

The majority of research and published documents have focussed on the fatigue performance of tubular welded joints and plates fabricated from conventional fixed offshore platform steels such as BS 4360 50D [1–9]. In addition, most corrosion fatigue tests conducted on offshore structural steels such as BS 4360 50D, BS 7191 355D were carried out at the most damaging wave operating frequency of 0.1–0.2Hz with cathodic protections [6–12]. Most of the experimental programmes [1–9] were undertaken two decades ago on the corrosion fatigue behaviour of fixed offshore platforms for oil and gas industry, where the natural frequencies are designed to be well above the wave excitation frequency. However, some of the works reported in literature have emphasised on the use of small scale test specimens for experimental investigation. This is due to their simplicity, relatively low cost, ability to simulate various numbers of variables and to determine useful fatigue data which can be extrapolated to real structures.

Scott et al. and Thorpe et al. [1,2] reported the corrosion fatigue crack growth behaviour of BS 4360 grade 50D steel in air and synthetic seawater using compact tension test specimen at a loading frequency of 0.1 Hz. Etube et al. [10] adopted a loading frequency of 0.2 Hz in a number of large scale corrosion fatigue tests to compare the fatigue behaviour of BS 4360 grade 50D and SE 702 steel. Constant amplitude fatigue test on welded joints fabricated from BS 4360 50D was investigated in air and in synthetic sea water at a loading frequency of 0.16 Hz [11], but it was observed that results based on conventional S–N approach were published as no fatigue crack growth data was reported. Vaessen and de Back [12] also conducted similar experiments as Booth [11] but they adopted a loading frequency of 0.2 Hz. Corrosion fatigue studies of welded joints fabricated from BS 4360 50D had also been extensively reported in the 1978 European Offshore Steels research seminar [6–12]. Majority of the published results have generally revealed that, at loading frequency of 0.1–0.2 Hz, seawater was detrimental to the fatigue performance of the joints and had also enhanced fatigue crack growth rates.

More recently, Griffiths and Turnbull [13] investigated the effect of exposure or soaking time to compare the corrosion fatigue crack growth of compact tension specimens that were extracted from AISI 4340 and BS4360 50D steels respectively. The tests on both materials were conducted at loading ratio of 0.167 Hz. Havn and Osvoll [14] also presented the effect of cathodic protection on crack growth rate of BS 4360 50D bar specimens at a loading frequency of 0.2 Hz in substitute ocean water prepared according to ASTM D1142-80.

Despite the number of research studies that have been conducted on offshore structural steels, there is still lack of proper understanding on the effect of corrosion fatigue on offshore wind turbine support structures. This paper documents the experimental assessment of crack growth rates of S355J2+N steel in a corrosive environment under various cyclic load frequencies in order to ascertain the effect of cyclic frequency of the applied loading within a frequency range pertinent to the reference structures. Comparison between the crack growth rates of S355J2+N steel and high strength steels data obtained under similar conditions are also established.

2. Overview of cyclic frequency for offshore wind turbine monopiles

Offshore wind turbines monopile structures are slender structures with more complex dynamic behaviour than the offshore platforms used in the oil and gas industry due to the added effect of operational loads from the rotor compared to what is obtainable in oil and gas platforms. It is also

essential to note that the loading regimes of offshore wind turbines differ entirely from that experienced by offshore oil and gas platforms; the first natural frequency of offshore wind turbines is considered dominant between wave and rotor load frequencies [15]. Studies have revealed that the support structures first order structural dynamic response lies in the range of 0.3–0.4 Hz [16–18]. This depends on a number of design factors such as monopile diameter and thickness, water depth, turbine size and soil conditions. However, what is not known is the extent to which corrosion fatigue crack growth rates in offshore wind farm monopile structures are influenced by cyclic load frequency across the relatively narrow band of frequencies reported in literature. This section provides a review of cyclic frequency for offshore wind turbines and the relevant references in this section informs the range of the test frequency used for testing.

Various researchers have investigated the dynamic response of offshore wind farm monopile structures. The DNV 2013 guideline on design of offshore wind turbine structures [19], stipulated that the natural frequency of wind turbine lies in a narrow band between the 1P and 3P frequencies which are specifically at least ±10% away from the 1P and 2P/3P frequencies. 1P and 3P are referred to as the rotor frequency and the blade passing frequency for a three-bladed wind turbine. During investigation on natural frequency of offshore wind turbines, there are three major design concepts which are considered based on soil conditions: the soft–soft, soft-stiff and stiff–stiff design approaches. The most commonly used is the 'soft–stiff' which stipulates that the natural frequency of the system lies between 1P and 3P [17]. These designs are often characterised based on soil structure interaction. Bhattacharya et al. [18] reported that the 1P and 3P values lie in the range of 0.115–0.2 Hz and 0.345–0.6 Hz respectively. In their study, it was concluded that for a 'soft–stiff' system, global fundamental frequency of a monopile was chosen to lie between 1P and 3P values in the range of 0.22 Hz and 0.31 Hz. Details of this are given in Ref. [18].

The first natural frequency of offshore wind farm monopiles was also reported to lie within the wide range of the rotor speed and blade passing frequency [20]. Using Horns Rev 1 Offshore Wind Farm as a reference case study, it was found that the first natural frequency based on different backfilling conditions are in the range of 0.279–0.293 Hz. This is in contrast to what was earlier reported by Bhattacharya et al. [18]. However, the fair difference in values was not accounted for in their study. Damgaard et al. [21], estimated the dominant cyclic frequency of an offshore wind turbine with a tower height of 60 m, on average water depth of 6/8 m and supported on a monopile of about 4.3 m in diameter to be 0.35Hz. In the Offshore wind turbines at exposed sites (OWTES) project, frequency sensitivity study of the response of offshore wind turbine supports based on data collected at Lely and Irene Vorrink offshore wind farms was studied [22] and the reported dominant first natural frequencies of the wind turbine was between 0.546 and 0.560 Hz from measurements while predicted values from finite element analysis was between 0.517 and 0.541 Hz respectively.

The dynamic response of offshore wind turbine monopiles based on results of three different wind turbine model packages was studied in Ref. [23]. They found that the dominant frequency of the system occurred at a peak of approximately 0.3 Hz. This value is in good agreement with some of the earlier reported findings. Adhikari and Bhattacharya [24] mentioned that, to avoid resonance type of failure of a 3 MW constant speed two-bladed Opti-OWECS wind turbine mounted on a soft-stiff system with 1P of 0.37 Hz and 2P of 0.74 Hz, the system should be designed for a natural frequency that lie between 0.37 Hz and 0.74 Hz. In their study, a mathematical model was used to predict the natural frequencies of A2-Lely and Irene Vorrink wind turbines to be 0.7404 Hz and 0.4565 Hz respectively as against the measured values of 0.634 Hz and 0.546 Hz. From their results, it can be noticed that there is a reasonable agreement between predicted dominant frequencies and the measured ones.

Camp et al. [22] estimated the natural frequency of Blyth (UK) Vestas V66 2 MW turbine to be 0.41 Hz while Carter [25] also predicted the natural frequency of North Hoyle (UK) Vestas V80 2 MW turbine to be 0.35 Hz. The soft-stiff system design approach was adopted in both cases and it can be observed that these values are reasonably close. Therefore, it can be concluded that the dominant frequency of the system can fall between these two reported values [21,24]. Andersen et al. [16] considered a simple model wind turbine supported on a monopile to estimate the natural frequency at 0.285 Hz. The response of the monopile structure with respect to wind and wave forces was not accounted for in their study, as this could reveal the difference in the estimated natural frequency compared to values earlier reported in this paper.

Considering the number of studies which have been mentioned in this paper on dynamic response of offshore wind turbines, it can therefore be concluded that the dominant cyclic frequency of offshore wind farm monopile support structures based on measurements and analytical investigations is averagely within the range of 0.3–0.4Hz. In order to investigate the effect of the aforementioned frequency loading in the seawater environment, tests have been conducted in this study and documented in this paper under free corrosion conditions using representative compact tension (CT) laboratory specimens.

3. Experimental programme

3.1. Material and specimen preparation

The material used for this experiment was EN10025-2:2004 S355J2+N. It should be noted that the chemical composition of the steel used does not fully comply with that of BS 4360:50D steel [1,2]. Reduction in phosphorus and sulphur content compared to what is available in 50D steel could result in significant changes in the fatigue response and this requires careful consideration. The thickness of the compact tension (CT) specimens was determined at 16 mm with the notch machined through spark erosion perpendicular to the rolling direction of the base metal plate. CT specimen dimensions were chosen based on preliminary calculation, considering the 100 kN capacity of the available loading machine and specification according to ASTM E647 [26] and BS EN ISO 11782-2:2008 [27] standards. Fig. 1 shows the design of the CT specimen.

Prior to experimental set up, the surfaces of the specimens were polished with 120, 400, 600 and 800 emery papers in ascending order in order to obtain a surface that is suitable for optical crack growth measurements.

3.2. Test procedure

3.2.1. Test setup

Fatigue crack propagation tests were carried out on two Instron 8801 100 kN servo-hydraulic fatigue test machines with digital controllers. The machines have an actuator stroke of ±75 mm. The procedure for testing was in accordance with [26,27]. Air tests refer to tests carried out at ambient conditions. The fatigue tests were carried out in load control to ensure constant load characteristics through the tests.

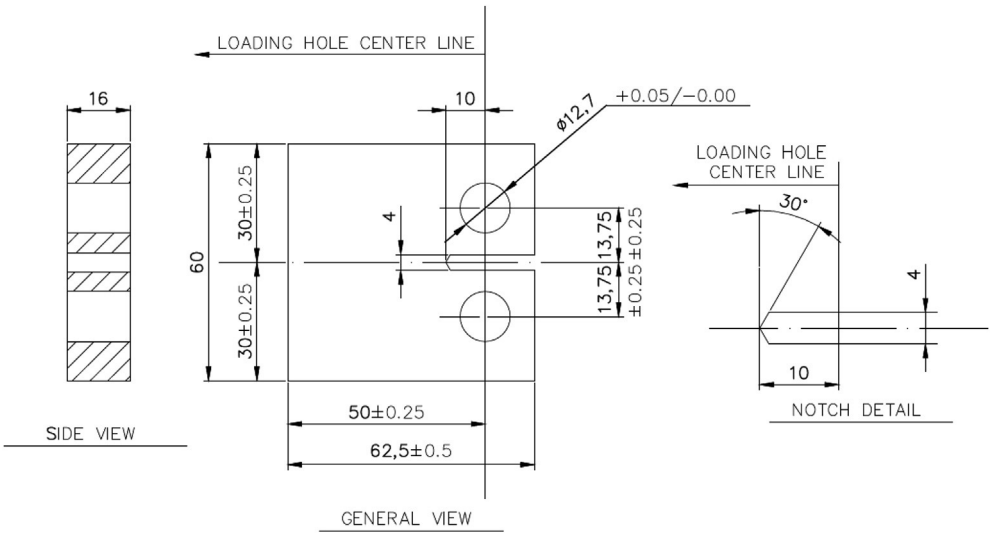

Fig. 1. Compact tension specimen design.

Prior to the commencement of the tests, the machines were checked for alignment through a purpose designed alignment tie. The three specimens tested in air were precracked to 4 mm maximum at a frequency of 5 Hz and load ratio of 0.1. The load was gradually reduced during the precracking process using the standardized procedure as set out in ASTM E647 [26].

Fatigue crack propagation was conducted through the application of constant amplitude sinusoidal loads on the specimens. Crack propagation data were obtained as a function of elapsed cycles at a load range of 10.8 kN and 9 kN, cyclic load ratio of 0.1 and a loading frequency of 2 Hz. Crack lengths were monitored by at least one or more of the four methods; Alternating Current Potential Difference (ACPD), direct current potential difference (DCPD), optical measurements through StreamPix5 digital camera and travelling microscope, and back face strain (BFS). The crack monitoring methods were validated with each other in air environment. The technique found particularly efficient here is the determination of crack length by BFS method in simulated seawater environment. Details of this will be given in a later section. Crack lengths were recorded with respects to the number of elapsed cycles and crack growth rates were determined from the plots of crack lengths a and elapsed cycles N using a seven point incremental polynomial method.

Cyclic crack tip stress intensity factor range ΔK was determined by the function of the form [26,27]:

$$\Delta K = \frac{\Delta P}{B\sqrt{W}} \frac{\left(2+\frac{a}{W}\right)\left(0.886+4.64\left(\frac{a}{W}\right)-13.32\left(\frac{a}{W}\right)^2+14.72\left(\frac{a}{W}\right)^3-5.6\left(\frac{a}{W}\right)^4\right)}{\left(1-\frac{a}{W}\right)^{1.5}} \quad (1)$$

Where;

ΔK is the stress intensity factor range, ΔP is the applied cyclic load range, B is the specimen thickness, W is the width of the specimen and a is the crack length.

3.2.2. Determination of crack length by the back face strain (BFS) method

The Back Face Strain (BFS) method was also employed as an alternative means of correlating crack lengths with optical measurements. The advantage of the back face strain method is its simplicity and relatively low cost compared to other crack lengths measurement methods. Care has been taken to produce the prediction curve in air based on optical measurements for validation. The unique difference in the BFS method presented in this paper compared to other BFS relations [28–31] which will be mentioned shortly is its ability to predict crack lengths in seawater environment. Linear Electrical Resistance Strain Gauges were installed at the back face of the specimens as shown in Fig. 2.

After the installation procedure, the lead wires were soldered to the strain gauge through the connecting terminals and the other ends of the wires were connected to a Vishay P3 strain indicator and recorder. The loading pattern of the strain gauged specimen within the loading grips of the machine is also illustrated (Fig. 2). The strain values and crack length from optical measurements were recorded as a function of elapsed cycles.

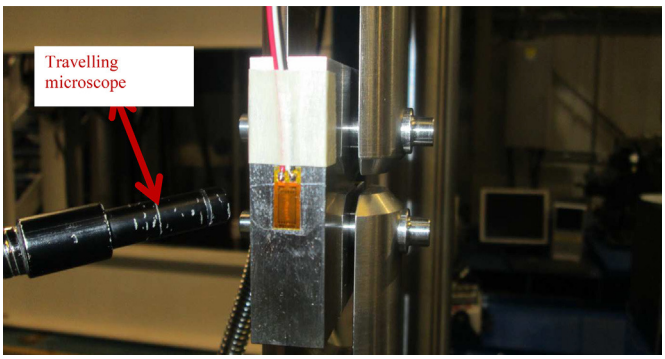

Fig. 2. Crack length monitoring by the back face strain method and travelling microscope.

3.2.3. Fatigue crack propagation in simulated seawater

The simulated seawater used for the corrosion fatigue test was prepared according to ASTM D1141 [32]. This was circulated past the CT specimen through the purpose designed and built Perspex Environmental chamber at a rate of 4 l/min, at a temperature of 8–10 °C and at a pH of 7.78–8.1. The experimental setup is shown in Fig. 3. The seawater environment was also regularly checked for salinity and oxygen concentration. It was ensured that the specimen was fully immersed in the seawater throughout the test period.

The CT specimens were precracked in air at a loading ratio of 0.1 and loading frequency of 5 Hz. The pre-cracked specimens were soaked for 48 h in the seawater before the commencement of the test to increase the corrosion fatigue crack growth rate. Constant amplitude sinusoidal loading was then applied to the specimens at a load ratio of 0.1; loading frequencies of 0.3, 0.35 and 0.4 Hz at different tests. Crack lengths were monitored by the Back Face Strain and DCPD methods and were recorded as a function of elapsed cycles. The strain gauges were protected against corrosion effect by coating the surfaces with N-1 coating material. The coating material is a Neoprene rubber material with an operating temperature of −30 to 80 °C and is suitable for protection against moisture and water. The coating material was applied over the strain gauges and under the lead wire in a thickness of about 1–2 mm.

4. Experimental results & discussion

4.1. Air test results

The results of fatigue crack growth rates of the S355J2+N steel in air in relation to crack monitoring methods and loading pattern of compact tension test (CT) specimens are shown in Figs. 4–9. Fig. 4 compares the ACPD technique with the optical methods for crack length measurements. Crack growth rates obtained with the aid of three independent crack measurement methods under the same loading conditions are shown together in Fig. 4. Here it can be seen that there is good agreement between the digital camera and the travelling microscope particularly at the threshold region. However, some disparities were observed between the two optical methods. This can be attributed to an error in the accuracy of the travelling microscope. An error of up to 31% was observed between the optical measurements and the ACPD method. This error is attributed to the sensitivity of the equipment to movement of the probes and the difficulty in obtaining a suitable injected field in such small-scale laboratory specimens.

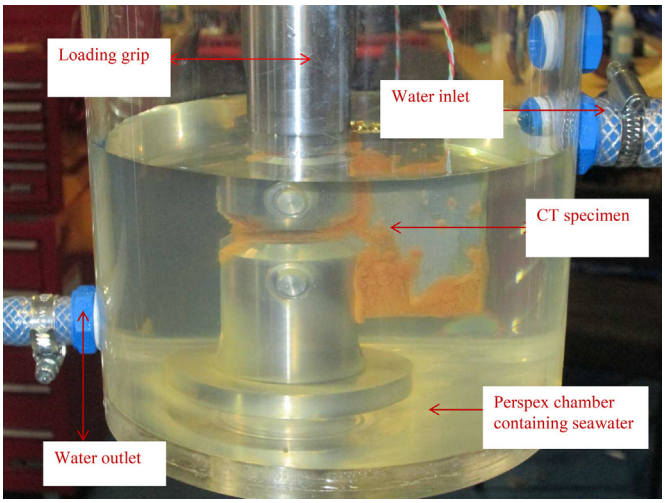

Fig. 3. CT specimen in simulated seawater.

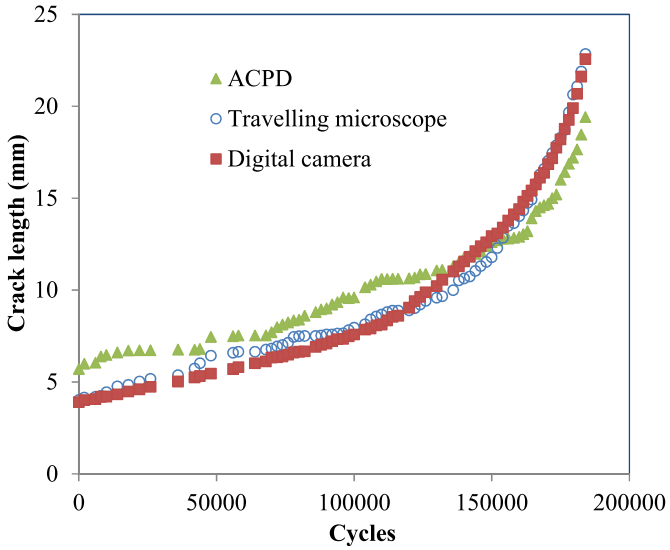

Fig. 4. Fatigue crack growth for CT specimens ($\Delta P = 10.8kN$).

The crack growth rate result is presented in Fig. 5 as a conventional plot of crack growth rates versus the cyclic Stress Intensity Factor Range. Crack growth rates were obtained at Cyclic Stress Intensity Factor Range (ΔK) of greater than 25 MPa$\sqrt{m}$. Since only the region II of the crack propagation test was considered in the present investigation, the experimental outcome of the crack growth data correlates well with the Paris law. This is described by a relationship of the form $\frac{da}{dN} = 4 \times 10^{-12}\Delta K^{3.20}$. The crack propagation results of the specimens tested at a load range of 9 kN using two types of waveforms; loop method and single wave matrix method are presented in Figs. 6–9. The difference between the two waveforms is the accumulated holding time in the loop method when the waveform is at mean load, a stage when the fatigue crack is fully open to allow reasonable strain and ACPD measurements. The

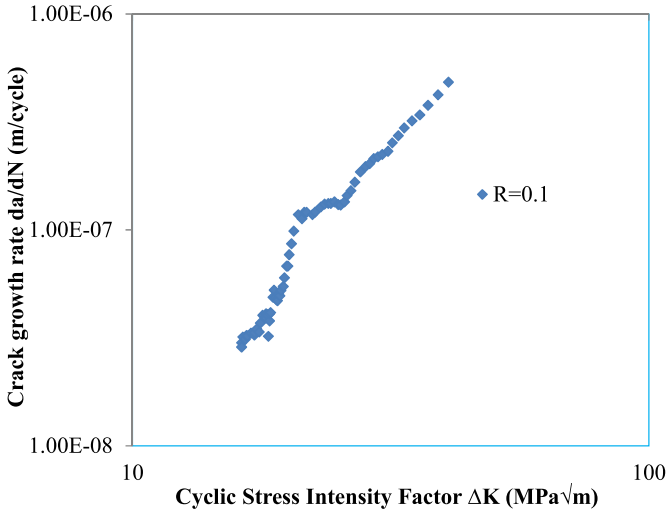

Fig. 5. Crack growth rate for CT specimens ($\Delta P = 10.8kN$).

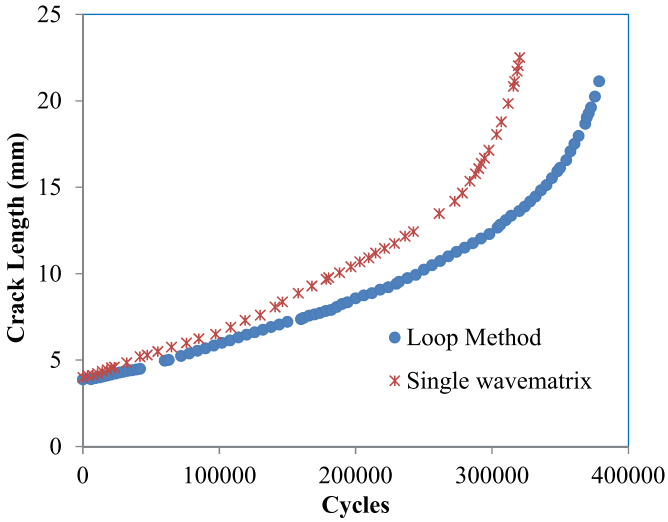

Fig. 6. Fatigue crack growth for CT specimens ($\Delta P = 9kN$).

single wave matrix method is the commonly used uninterrupted sinusoidal waveform for fatigue crack propagation. In the loop method, a loop was created to repeat several times based on the total number of cycles for the test. In each loop, the wave matrix was programmed to hold for few seconds at the test mean load after the desired number of cycles has been applied through the sinusoidal waveform. This method was written in the wave matrix software in order to minimise any deviation in the ACPD and strain gauge outputs.

Crack propagation data were recorded over 330,000 cycles for the single wave matrix method, while the specimen tested at loop control waveform extended over 374,000 cycles despite the similarity in loading conditions for both specimens. The disparity in the number of cycles experienced in the specimens could be attributed to the effect of accumulated waveform interruption in the loop

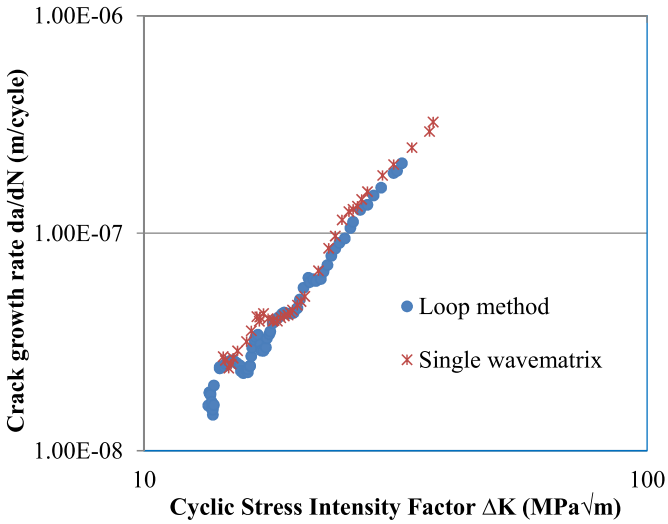

Fig. 7. Crack growth rate for CT specimens ($\Delta P = 9kN$).

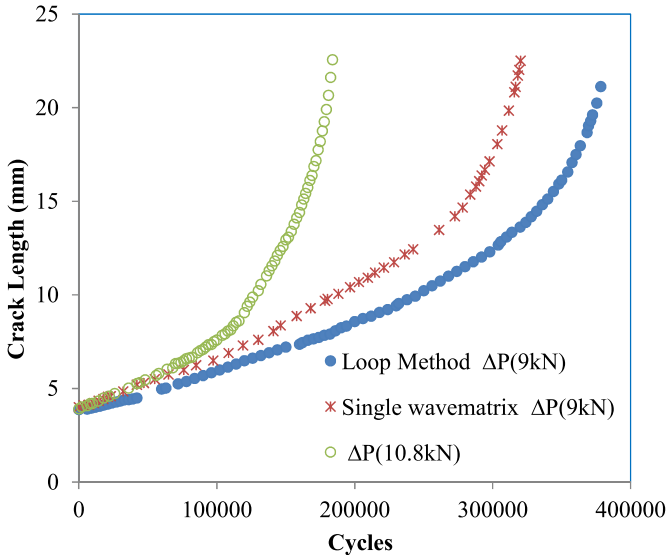

Fig. 8. Comparison of fatigue crack growth in air at different loads.

control method as earlier mentioned. Crack growth rates for the specimens were obtained at ΔK of 19 MPa$\sqrt{m}$ and 23 MPa$\sqrt{m}$ respectively. It may be noted that the loading pattern of the specimens did not have a major effect on the crack propagation results. Consequently, theΔK crack growth data for the specimens tested at a load range of 9 kN were represented by $\frac{da}{dN} = 1.0 \times 10^{-11}\Delta K^{2.8}$ for loop control waveform and $\frac{da}{dN} = 1.1 \times 10^{-11}\Delta K^{2.8}$ for single wave matrix. Figs. 8 and 9 compares the result of the effect of load range and loading pattern on the three tested specimens, illustrated on conventional plots of crack length versus number of cycles and crack growth rates ($\frac{da}{dN}$) versus stress intensity factor range (ΔK) respectively.

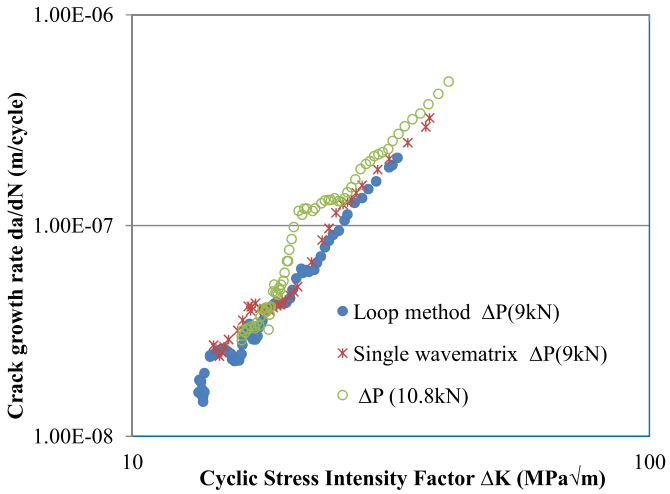

Fig. 9. Crack growth rate in air at different loads.

An increase in crack propagation rates is clear due to an increase in applied load range within all the applied range, as shown in Figs. 8 and 9. This is also evident in the test data plotted in Fig. 8; a significant effect of load range was shown by a factor of approximately 2 in the number of loading cycles at higher relative to lower ΔP. It was also observed from the experimental data that, higher ΔK values were obtained at a higher load range than the lower one as should be expected. The result of the present investigation compared well with those obtained using 37.5 mm CT specimen from similar material [1,2]. Table 1 summarises the loading parameters of the specimens and the material constants. The result of the test carried out on CT specimens from the same plate; subjected to different loads and loading patterns are presented for comparison. The notable test variable here is the applied load range (ΔP). Also included in Table 1 are values of the multiple correlation coefficients resulting from the line of best fit through the $\frac{da}{dN}$ versus ΔK plots. The fitting is satisfactory considering that all the determined coefficients correspond to R^2 values of above 95%, which represents a good fit.

4.2. Back face strain regression expression for prediction of crack lengths in corrosive environment

Back face strain (BFS) compliance relationship was used in the study to predict crack length as a function of elapsed cycles in a simulated seawater environment at a temperature between 8-10 °C. BFS represents the compressive strain measured at the back face of specimens along which the notch is machined as shown in Fig. 10. The purpose of the strain gauge is to detect the strain values as the fatigue crack propagates through the specimen. The most commonly used compliance relation to crack lengths is the crack mouth opening displacement (CMOD) technique [26]. The method involves monitoring of crack lengths by measuring the displacement at the front face of the specimen through an inserted CMOD gauge. The standardized procedure is outlined in the ASTM E647 [26] but a BFS relation to optical measurements is not included yet and has not been reported. The CMOD/BFS have been extensively used for prediction of wide range in crack lengths for small laboratory specimens such as CT and four-point bend specimens. Deans and Richards [28] developed BFS crack length compliance equation for CT specimen using the CMOD technique. Their proposed relationship was valid for $0.1 \leq a/W \leq 0.7$. A finite-element code (FRANC2D) was employed by Riddell & Piascik [29] to develop a compliance relation for CT specimen that is valid for $0.1 \leq a/W \leq 0.9$. Though, their compliance equation was expressed in logarithmic form compared to other linear relations which will be mentioned shortly in this paper.

A BFS- crack length calibration equation in the range $0.2 \leq a/W \leq 0.7$ was also developed by Shaw and Zhao [33] using CT specimens that were manufactured from aluminium alloy. Huh and Song [30] reported the BFS relation for four-point bend specimen through finite element analysis and experimental studies. The validity of their calibration equation was $0.15 \leq a/W \leq 0.6$ and reasonable agreement was achieved between the two methods. Recently, Newman et al. [31] determined a BFS-crack length compliance relationship for CT specimens using the FRANC2DL; a finite element code and FADD2D; a boundary element code which is valid over crack length to width ratio of 0.1–0.95. Their result is somewhat similar to the ones published by Riddell and Piascik [29]. As earlier mentioned, the major observed difference was log functional BFS relation they developed.

In this study, a mathematical expression has been developed for monitoring crack lengths based on optical measurement on a $W = 50$ mm specimen. The reliability of the compliance relationship here has been demonstrated for prediction of crack lengths in corrosive environment Fig. 11 shows a plot of crack lengths and BFS.

Using the approach described in the ASTM E 647 [26], the relationship between force versus displacement slope normalised for modulus of elasticity, specimen thickness and crack length for several standard specimens have been expressed as a relationship of EvB/P and the normalised crack

Table 1
Loading scenarios and material constants for S355J2+N steel in air.

ΔP (kN)	R	C	m	R^2
10.8	0.1	4.1×10^{-12}	3.2	0.95
9 (Loop)	0.1	1.0×10^{-11}	2.8	0.98
9 (Single)	0.1	1.1×10^{-11}	2.8	0.97

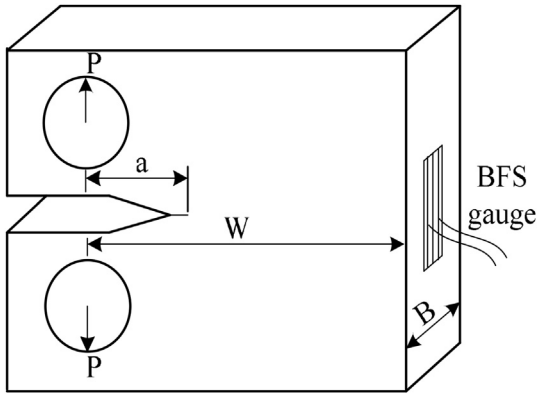

Fig. 10. Compact tension specimen with BFS gauge.

length a/W [26], [31]. Where V is the Crack Mouth Opening Displacement (CMOD). The relationship in this paper is formulated by replacing V with the absolute strain multiplied by the specimen width and by correlating the optically measured crack lengths with BFS. The mathematical expression is represented by the polynomial equation of the form:

$$a/_W = C_0 + C_1U + C_2U^2 + C_3U^3 + C_4U^4 + C_5U^5 \tag{2}$$

Where $a/_W$ is the crack length to width ratio and C_0 to C_5 are the regression coefficients which depends on crack length to width ratio.

$$U = \left[(|EB\varepsilon W|/P)^{1/2} + 1\right]^{-1} \tag{3}$$

Where $|EB\varepsilon W|/P$ is a dimensionless back face strain parameter which is represented in literature [29]. E is Young's modulus, B is thickness, ε is the strain and P is applied load. The regression coefficients for 0.2< a/W < 0.65 which is considered in this study based on W = 50 mm specimen are:

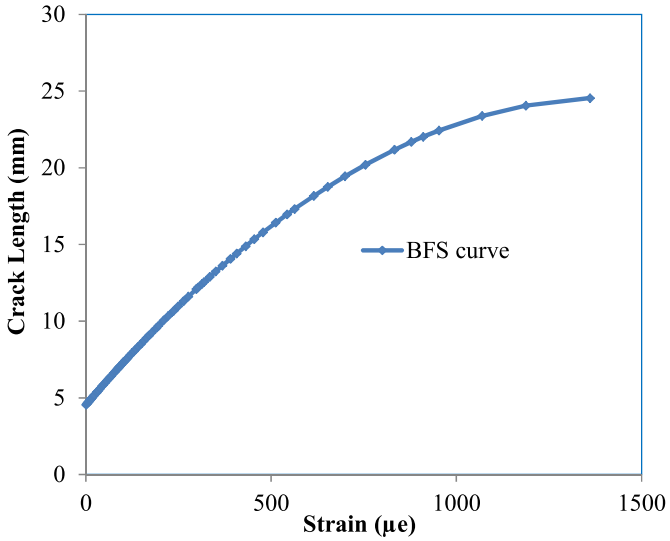

Fig. 11. Crack lengths versus back face strain.

$C_0 = 0.4427\ C_1 = -3.4995\ C_2 = 15.925$

$C_3 = -37.93\ C_4 = 39.313\ C_5 = -12.9123$

Within the range of validity of the present mathematical relation, the polynomial expression fits the data point obtaining a correlation coefficient of approximately 1.The result of the strain normalising parameter is displayed in Table 2 as a comparison with other published compliance relations. Fig. 12 also compares this study with other reported BFS relations considering results which fall within the range of validity of the present expression. Variations in presented results may be attributed to specimen dimensions, applied load and the properties of the material. The range of validity of BFS relation in this paper is a function of the specimen width (W = 50 mm) and the remaining uncracked ligament which has to be carefully monitored without fracturing the specimen. Deans and Richards results agree fairly well with the present result except at a/W ratios of 0.55–0.65. Riddell and Piascik results were somewhat similar but it could be noted that some intermediate results were not given within the range of the validity of their proposed equation.

Newman et al. [31] relation gave a closer result based on the considered a/W ratio in the present equation. The difference in the applied range here compared to the work of Newman et al. is a function of the specimen width. As earlier mentioned it is interesting to note that there are no available optical or visual crack lengths versus measured back face strain. The relation here has been compared with other CMOD and numerically derived relations to justify the accuracy of the present method (Fig. 12). Prediction of crack lengths through protected strain gauges have also been demonstrated in corrosive environment at low temperature using the present BFS relation to obtain good agreement with other crack length measurement methods.

4.3. Seawater test

Corrosion fatigue crack propagation tests were conducted in seawater under free corrosion conditions on three pre-cracked CT specimens at a load range of 9 kN and 12 kN; loading frequencies of 0.3,0.35 and 0.4Hz respectively. Crack lengths were monitored with back face strain and DCPD

Table 2
Back face strain parameter versus a/W.

$\lvert EB\varepsilon W\rvert/P$					
a/W	Riddell & Piascik (1998)	Deans & Richards (1979)	Shaw &Zhao (1994)	Newman et al. (2011)	Present study
0.1	1.803	–	–	1.783	–
0.15	–	–	–	2.162	–
0.2	2.71	–	3.002	2.704	2.707
0.25	–	–	3.405	3.449	3.453
0.3	4.436	4.26	4.492	4.443	3.995
0.35	–	5.56	5.999	5.742	5.227
0.4	7.422	7.17	7.868	7.437	7.093
0.45	–	9.31	10.24	9.66	9.296
0.5	12.581	12	13.461	12.62	12.376
0.55	–	15.6	18.076	16.66	16.501
0.6	22.197	20.6	24.834	22.35	23.008
0.65	–	27.8	34.687	30.74	28.840
0.7	43.003	38.3	48.787	43.83	–
0.75	–	–	–	65.93	–
0.8	100.076	–	–	107.3	–
0.85	–	–	–	198	–
0.9	420.5	–	–	460.1	–
0.95	–	–	–	1809	–

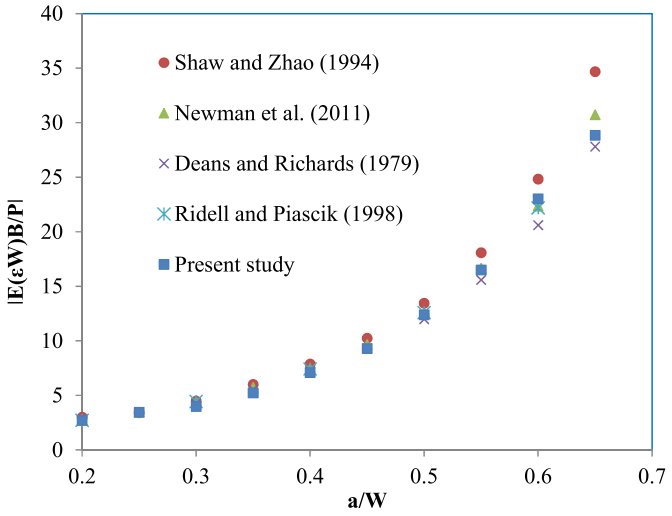

Fig. 12. Calibration curve for crack lengths and back face strain.

methods. Fig. 13 shows the DCPD calibration curve. The data points were fitted by a polynomial equation of the form

$$a = -7 \times 10^{-6} v^2 + 0.0474v - 52.276 \tag{4}$$

Where a is the crack length and v is the active voltage. Both crack length prediction curves; BFS and DCPD were used to monitor crack lengths in air and seawater using the previously reported test parameter for the air test. The results are presented in Figs. 14–19. Fig. 14 compares BFS and DCPD results with optical measurements and it can be seen that a reasonable agreement was achieved.

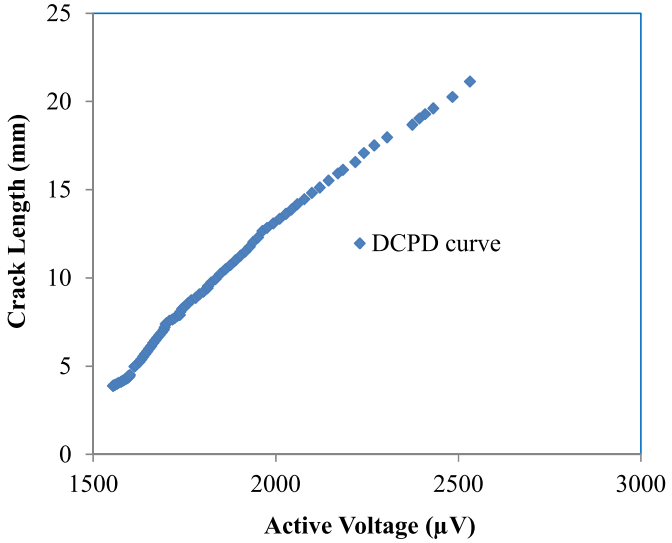

Fig. 13. DCPD voltage and crack length calibration curve.

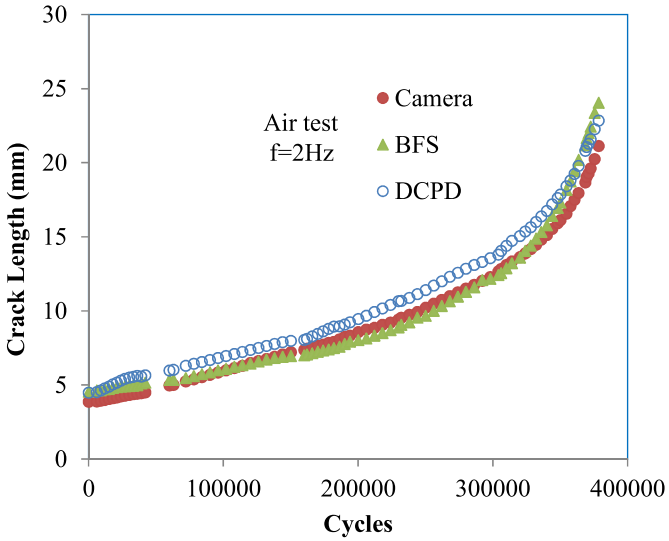

Fig. 14. Fatigue crack growth in air at a frequency of 2 Hz.

The air and seawater test results are compared in Figs. 15 and 16, showing the crack growth data in air and seawater under free corrosion conditions. Results generally revealed that, crack growth rates are faster in seawater than in air. This is evident in Figs. 15 and 16 by an increase in crack growth rate by a factor of approximately 2 in seawater compared to air regardless of the test frequencies and the loading conditions.

The crack growth plot in Fig. 16 was obtained from the crack length versus number of cycles data using the incremental polynomial method. The air and the free corrosion seawater test data when analysed correlates well with the Paris law. Comparing the data revealed that, at higher ΔK crack growth rate in seawater was faster than in air but at lower ΔK, the behaviour was somewhat similar. The

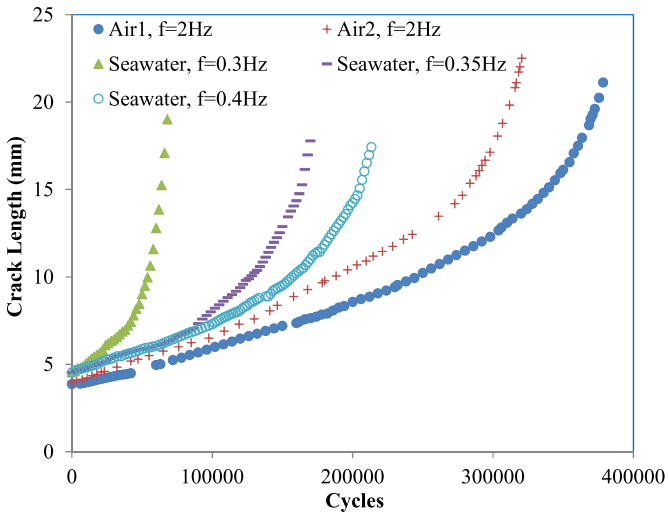

Fig. 15. Comparison of fatigue crack growth in air and seawater.

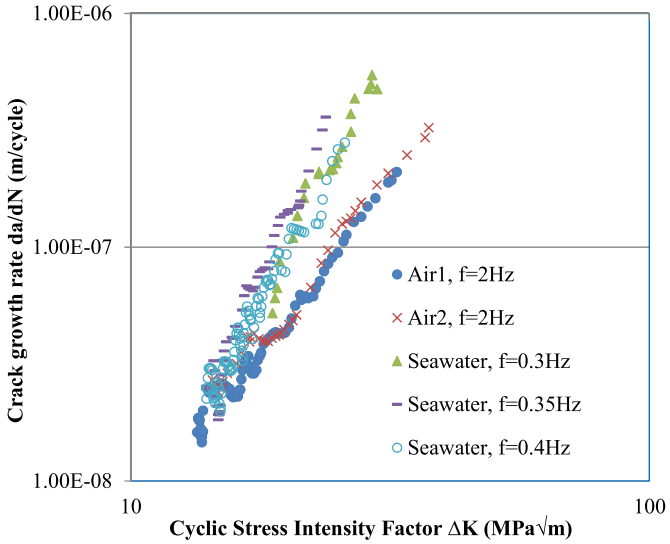

Fig. 16. Comparison of crack growth rate in air and seawater.

underlying reason for this could be attributed to the time dependent phenomenon of corrosion fatigue which becomes pronounced at lower frequencies as the crack propagates through the specimen. Also, at R ratio of 0.1, the test load range may not be fully effective at lower frequencies and at lower number of loading cycles. At ΔK 13 MPa$\sqrt{\text{m}}$, the $\frac{da}{dN}$ in seawater is approximately 2 times that of air. The results show the crack growth plateau in the range of 13–25 MPa$\sqrt{\text{m}}$. At higher ΔK, the crack growth rate is increased by a factor of approximately 4 in seawater than in air. This was observed at ΔK of 24 MPa$\sqrt{\text{m}}$ in both cases. It is also interesting to note that the specimen tested in seawater exhibited a higher crack growth rate just after the near threshold region at approximately the same ΔK as in air. The explanation for this may be due to the effect of pre-exposure period of 48 h to the corrosive environment prior to test.

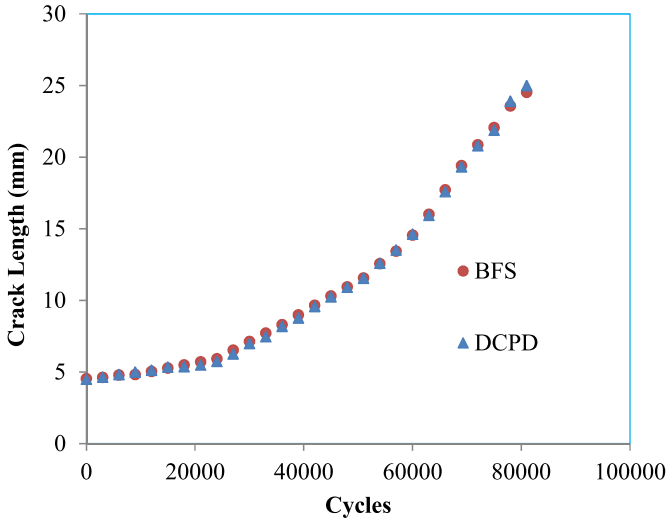

Fig. 17. Comparison of fatigue crack growth in air with DCPD and back face strain.

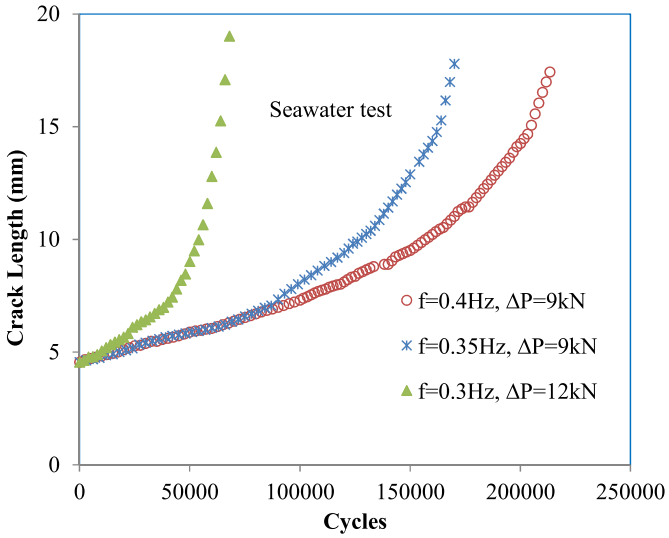

Fig. 18. Comparison of fatigue crack growth in seawater at different loads and frequencies.

This could also be attributed to the time dependent accumulation of the simulated salt water as this may have a profound effect on crack tip of the specimen prior to the start of the experiment. Generally, from the seawater data, it was observed that better fatigue response was exhibited due to the reduction in experimental scatter compared to results from the similar material [1,2].

Fig. 17 compares *DCPD* and BFS results. From the analysis, there is a good agreement between both crack monitoring methods and this reflects the accuracy of the crack length BFS relation. Seawater tests conducted at loading frequencies of 0.3 Hz and 0.35 Hz and 0.4 Hz are plotted together and are presented in Figs. 18 and 19.

The effect of different load frequencies and load range are compared on the measured crack growth rates in Figs. 18 and 19 to establish a sensitivity analysis of the test load frequencies. Similar crack growth behaviour is demonstrated from the three load frequencies especially at lower load cycles as

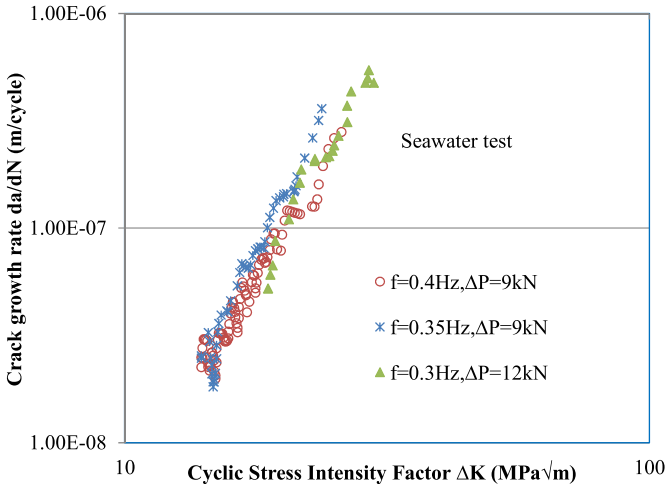

Fig. 19. Crack growth rates in seawater under different loading conditions.

indicated in Fig. 18. Crack propagation data based on the test frequencies were parallel over a substantial range of load cycles but was pronounced between load frequencies of 0.35 and 0.4 Hz, regardless of the difference in test frequencies. The profound effect of seawater environment and test frequency was not dominant at 0.35 Hz until nearly 30% of the total number of cycles was expended compared to what was experienced at 0.4 Hz. This behaviour could be attributed to the effect of seawater which progressively manifests at an increased crack opening displacement and subsequent increase in ΔK at each fatigue cycle. However, this was in contrast to the crack growth behaviour at 0.3 Hz due to the high load range. As such, the testing time was reduced as much as half of the time taken using lower load. In Fig. 19, the three cases are plotted together as a comparison. The crack growth rates for the tests were obtained at ΔK of 11 MPa$\sqrt{}$m. At lower ΔK, the crack growth rates are similar but at higher ΔK, the crack growth rate at frequency of 0.35 Hz was twice that of 0.4 Hz. At an intermediate ΔK of 18 MPa$\sqrt{}$m, the crack growth rates for the three cases are somewhat similar regardless of the difference in test conditions. It is also interesting to note that higher value of ΔK_{th} was exhibited in the seawater test than that in air. A higher ΔK_{th} was also reported for BS4360 50D steel at R ratio of 0.1 in a free corrosion condition [34–36]. This effect was attributed to crack closure effects at lower R ratios and particularly at an R ratio of 0.1 but at an R ratio of 0.7, the effect disappeared and produced the same ΔK_{th} as in air.

This is due to the fact that for tests conducted at higher R ratio, the crack surfaces do not touch during the unloading part of the stress cycle but this is not studied in this paper. The change in load range had an obvious effect on the crack growth data as would be expected (Fig. 19). The results generally reveal that there was a considerable reduction in fatigue propagation life, up to a factor of 3 in specimen tested at a higher ΔP and lower frequency than the one tested at lower ΔP and higher frequency. Table 3 summarises the loading variables of the specimens, the Paris constants and the correlation coefficients.

5. Fatigue crack growth results comparison

Fatigue crack growth data have been rarely obtained in free corrosion conditions under representative wind and wave load frequencies such as the ones reported in this paper and it should be mentioned that the environmental condition under a free corrosion potential is different from a free corrosion condition. This is because a free corrosion potential environment is a simulated free corrosion condition which is likely to be associated with hydrogen production due to cathodic reactions. This may result in some levels of hydrogen embrittlement at the crack tip, a proportion of which depends on the level of protection and the type of material. It was mentioned that the mechanism associated with crack growth rates in a free corrosion condition can be explained by anodic dissolution [37]. However, the fact that a free corrosion condition is primarily associated with anodic dissolution of steels by corrosion does not imply that the same process will occur under a free corrosion potential which have been demonstrated in most investigations earlier mentioned in this paper. This requires a careful consideration when results are being interpreted. Also, previous published data, for example in Refs. [1] and [2] have categorised different levels of applied cathodic protections of −0.6V, -0.85V and −1.3V potentials with reference to Ag/AgCl electrodes as free corrosion, normal protection and over protection potentials. Another important factor that should be noted from result comparison is that modern steels such as S355J2+N steel have improved properties such as toughness and weldability compared with the BS4360 50D steels due to the reduced levels of carbon and the additions of other elements.

Table 3
Loading scenarios and material constants for S355J2+N steel in seawater.

Δ**P** (kN)	f	C	m	R^2
12	0.3	1.1×10^{-13}	4.5	0.95
9	0.35	2.3×10^{-14}	4.9	0.96
9	0.4	5.2×10^{-13}	4.0	0.96

The results of the present investigation are compared with data taken from literature and with recommendations in the BS7910. The results comparison is classified based on data obtained from offshore structural steels with yield stresses in the region of 350–900 MPa. Steels used for offshore structures have been categorised into conventional steels (yield strength of about 350 MPa), high strength steels (yield strength of 400–600Mpa) and extra high strength steels used in ships and Jack – up platforms (yield strength of 700–900 MPa) [38]. Fig. 20 compares the results of fatigue crack response of the steels used in this work with other similar medium strength steels such as BS4360 50D and C–Mn–V steels [1,2,14,39].

The air data are plotted on the left of Fig. 20 while the seawater data are compared on the right. The results of the air tests showed a similar trend to that of Thorpe et al. [2] over the stress intensity factor ranges. Fukuda et al. [39] and Havn and Osvoll [14] results deviates from the present results particularly at lower $\Delta \boldsymbol{K}$ and resulted in bi-linear trends, with Havn and Osvoll data having approximately twice the crack growth rates obtained in S355J2+N steel at $\Delta \boldsymbol{K} > 27$ MPa$\sqrt{}$m. The response from S355J2+N steel also shows a significantly reduced scatter compared to Thorpe et al. data. The use of nowadays better fatigue data acquisition techniques compared to those used in the 1970s and 1980s could be a contributing factor to the reduction in experimental scatter. However, from the overall comparison of the air data, the most similar propagation behaviour to S355J2+N steel is the data obtained from BS4360 50D steel.

The crack growth rates in seawater plotted in the right of Fig. 20 is the mean data obtained at the three examined cyclic load frequencies. It can been seen that the present data are reasonably closely matched compared to the significant scatter derived from Thorpe et al. data [2]. Thorpe et al. results were obtained at a test frequency of 0.1Hz while that of C–Mn–V steel were obtained at 0.133Hz. It can be seen that crack growth curves from the two materials are parallel while the present mean data lies between the two curves and Havn and Osvoll data that was obtained at 0.2Hz. However, the difference in crack propagation behaviour in Havn and Osvoll studies particularly at lower $\Delta \boldsymbol{K}$ compared to the others curves may be probably due to the effect of test load range. Also, it should be mentioned that fatigue crack propagation behaviour is not only load or cyclic frequency dependent but is also material dependent. However, overall observation in seawater as shown in the right of Fig. 20 revealed that the crack growth trend in the present investigation agrees fairly well with the other curves plotted in the Figure.

In Fig. 21, the crack growth rates of S355J2+N steel are compared in air and in seawater with crack growth rates in high strength steels such as pipelines and offshore platforms steels (C–Mn, API X70, API X65 and RQTuf 501) in the region of 400–600Mpa [40–43]. It can be seen in the left of Fig. 21 that the crack growth trends of S355J2+N steel is similar to that of the high strength steels, but crack growth rates are higher in the three other steels than that reported by Bertini [40] for a C–Mn steel. Crack growth rates in S355J2+N steel also falls within the growth rates in API X70 [42], API X65 [43]and RQTuf 501 [41]

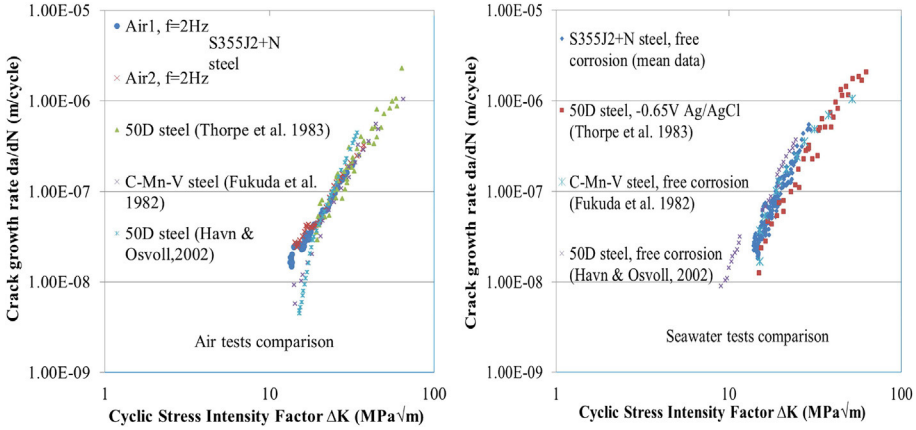

Fig. 20. Comparison of fatigue crack growth in air and seawater with medium strength steels.

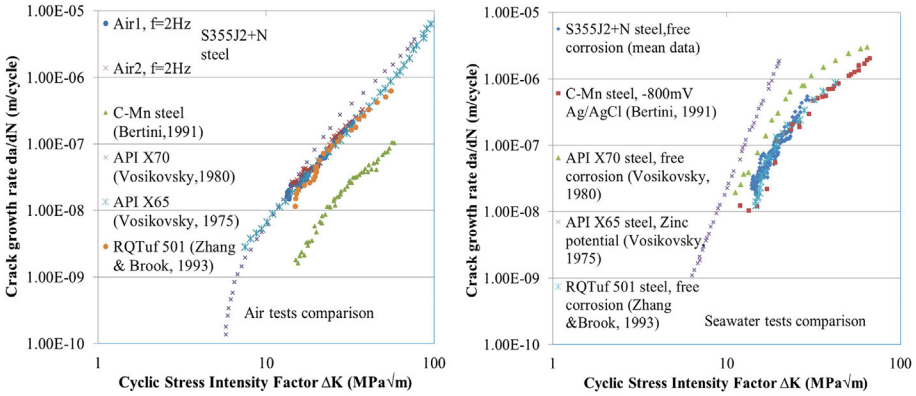

Fig. 21. Comparison of fatigue crack growth in air and seawater with high strength steels.

steels. It is also seen that the crack growth rates in API X70 are higher than in API X65 particularly at higher ΔK. Though, S355J2+N steel has a lower yield strength than API X65, API X70 and RQTuf 501 steels but a significant effect of this is not seen in their responses as shown in the air comparison plots. It can be admitted that the C–Mn steel has a better performance in air than the other steels.

However, their performances in seawater are different compared to in air as shown in right of Fig. 21. The crack growth rates are similar except for the results reported by Vosikovsky [43] for an API X65 steel under zinc potential. This implies that environmental tests conditions for each of the steels may probably contribute to the observed crack growth rates. There is also a noticeable effect of the corrosive environment in the crack growth rates of C–Mn compared to the behaviour in air due to the associated effective mechanisms in promoting crack growth rates in seawater compared to in air. Despite the optimum protection of −800 mV that was offered to C–Mn steel, it can be seen that there is no marked difference in the crack growth rates compared with the responses from S355J2+N and RQTuf 501 steels respectively. This also implies that the performance of S355J2+N in seawater environment is similar to that of C–Mn steel and RQTuf steels regardless of its lower yield strength. It can also be observed form Fig. 21 that crack growth rates are higher in API X65 and API X70 steels than the other steels compared. The deviation in crack growth rates in API X65 is significantly higher in seawater environment compared to their responses in air probably due to the differences in corrosion potential and yield stress.

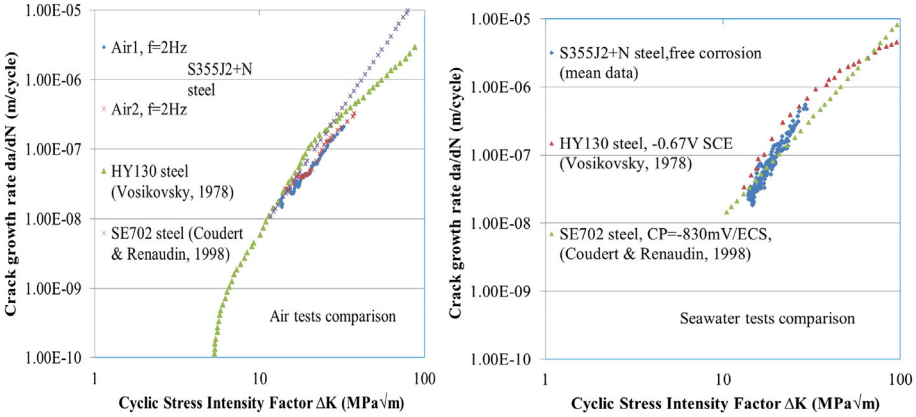

Fig. 22. Comparison of fatigue crack growth in air and seawater with extra high strength steels.

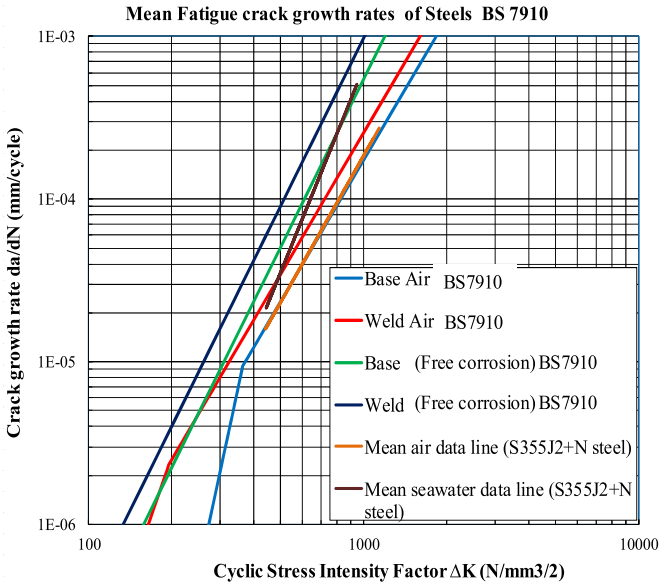

Fig. 23. Comparison of fatigue crack growth in air and seawater with BS7910 recommendations.

Fig. 22 compares the fatigue crack growth of S355J2+N steel with that of HY 130 [44] and SE702 [45] steels in air and in seawater. The S355J2+N steel shows better resistance to fatigue crack growth compared to HY 130 and SE702 steels in air as shown in the left of the Figure. The crack growth behaviour of HY 130 steel shows a bump shape particularly at intermediate levels of ΔK, while at higher ΔK, the curve almost converged with that of S355J2+ N steel. At lower ΔK in air, the crack growth rates in S355J2+N steel is similar to SE702 steel but at higher ΔK, the crack growth rate is twice higher than in S355J2+N steel. The seawater comparison is plotted on the right of Fig. 22. The crack growth behaviour of the steels are similar at lower ΔK, while at higher ΔK, crack growth rates in HY 130 steel is slightly higher than the other two steels and curve converged with that of SE702 steel. An optimum cathodic protection of −830mV/ECS was applied to the SE702 steel, so it is expected that the resistance to the detrimental effects of corrosion will be typically more evident but the effect of the cathodic protection is not noticeable particularly at lower ΔK. Crack growth rates in S355J2+N steel is slightly lower than that of SE702 and HY 130 steels but at higher ΔK, majority of the data points are between the SE702 and HY 130 curves. Overall comparison of the crack growth behaviour of S355J2+N shows a similar and in some case better behaviour than the crack growth rates in the different grades of steels compared in this paper. It appears that there is a potential benefit in using S355J2+N compared to high strength steels for offshore applications.

The results of crack growth rates in S355J2+N steel in air and seawater are compared to the BS7910 recommendations [46] as shown in Fig. 23. The mean air and seawater data lines are plotted in the Figure. The mean data lines are in accordance with the recommendations as shown in the Figure, but the air data comparison with the design curve appears better than that of the seawater. However, the mean seawater data line generally lies within the acceptable region of the recommended free corrosion design curve for base materials.

6. Conclusions

This paper documents the development of a test procedure for the calculation of crack growth rates in free corrosion seawater conditions and investigated whether any appreciable difference was apparent between cycling at 0.3 Hz and 0.4 Hz. A BFS relation was developed for prediction of crack lengths in a laboratory simulated seawater environment. The following conclusions can be drawn:

- Within a Stress Intensity Factor Range of 16–50 MPa$\sqrt{m}$ Crack Growth Rates of the corrosion tests are seen to be faster than the rates observed for air but at lower values of K generally no more than twice the equivalent air test;
- There was no consistent trend observed indicating a more severe situation at a slower cyclic frequency 0.3Hz compared to cyclic load frequencies of 0.35Hz and 0.4 Hz. The seawater tests showed that similar crack growth rates were exhibited using the three test frequencies regardless of load range. However, the differences were small and within experimental scatter;
- ACPD was shown to be unsuitable for crack growth monitoring in CT test specimens;
- DCPD and Back Face Strain measurements were seen to be reliable and cost-effective methods for crack growth measurement in a corrosion environment where optical measurements are not applicable;
- The fatigue crack growth behaviour of S355J2+N steel was shown to be similar and in some cases better than that of different types of high strength steels used for offshore installations;
- The fatigue growth behaviour of S355J2+N steel in air and seawater was in accordance with the BS7910 recommendations.

Acknowledgements

The authors acknowledge the support of the Offshore Wind Structural Lifecycle Industry Collaboration (SLIC) project managed by Centrica Energy (UK) Ltd and of the Petroleum Technology Development Fund (PTDF), Nigeria who support the PhD of Oyewole Adedipe.

References

[1] Scott PM, Thorpe TW, V Silvester DR. Rate -determining process for corrosion fatigue crack growth in ferrite steels in seawater. Corros Sci 1983;23(6):559–75.
[2] Thorpe TW, Scott PM, Rance A, Silvester D. "Corrosion fatigue of BS 4360:50D structural steel in seawater. Int J Fatigue Jul. 1983;5(3):123–33.
[3] Wildschurt H, de Back J, Dortland W, Van Leeuween JL. Fatigue behaviuor of welded joints in air and sea water. Paper 5 in European Offshore Steels research seminar. 1978.
[4] Haagensen PJ, D'Erasmos P, Petterson B. Fatigue performance in air and sea water and fracture of TIG-dressed steel weldments. Paper 8 in European Offshore Steels research seminar. 1978.
[5] Booth GS. Fatigue and corrosion fatigue of welded joints under random loading conditions. Paper 9 in European Offshore Steels research seminar. 1978.
[6] Berge S. Constant amplitude fatigue strength of welds in a sea water drip. Paper 12 in European Offshore Steels research seminar. 1978.
[7] Solli O. Corrosion fatigue of welded joints in structural steels and the effect of cathodic protection. Paper 10 in European Offshore Steels research seminar. 1978.
[8] Bardall E, Sondenfor JM, Gartland PO. Slow corrosion fatigue crack growth in a structural steel in artificial sea water at different potentials, crack depths and loading frequencies. Paper 16 in European Offshore Steels research seminar. 1978.
[9] Haagensen PJ, Dagestad V. Random load crack propagation in seawater in a medium- strength structural steel. Paper 22 in European Offshore Steels research seminar. 1978.
[10] Etube LS, Myers P, Brennan FP, Dover WD, Stacey A. Constant and variable amplitude corrosion fatigue performance of a high strength jack-up steel. In: International offshore and polar engineering conferenceIV; 1998. p. 123–30.
[11] Booth GS. The influence of simulated north sea environmental conditions on the constant amplitude fatigue strength of welded joints. In: Offshore technology conference; 1979. p. 547–51.
[12] Vaessen GHG, de Back J. Fatigue behaviuor of welded steel joints in air and seawater. In: Offshore technology conference510; 1979. p. 555–8.
[13] Griffiths AJ, Turnbull A. Impact of long term exposure on corrosion fatigue crack growth of alloy steels. In: NACE International annual conference and exposition; 1996. p. 2–9.
[14] Havn T, Osvoll H. Corrosion fatigue of steel in seawter. 02431. In: NACE international corrosion conference; 2002. p. 1–11.
[15] Zaaijer MB. Foundation modelling to assess dynamic behaviour of offshore wind turbines. Appl Ocean Res Feb. 2006;28(1):45–57.
[16] Andersen LV, Vahdatirad MJ, Sichani MT, Sørensen JD. Natural frequencies of wind turbines on monopile foundations in clayey soils—A probabilistic approach. Comput Geotech Jun. 2012;43:1–11.
[17] Lombardi D, Bhattacharya S, Muir Wood D. "Dynamic soil–structure interaction of monopile supported wind turbines in cohesive soil. Soil Dyn Earthq Eng Jun. 2013;49:165–80.
[18] Bhattacharya S, Nikitas N, Garnsey J, Alexander NA, Cox J, Lombardi D, et al. Observed dynamic soil–structure interaction in scale testing of offshore wind turbine foundations. Soil Dyn Earthq Eng Nov. 2013;54:47–60.
[19] Det Norske veritas. DNV-OS-J101: design of offshore wind turbine structures. 2013.
[20] Peder Hyldal Sørensen S, Bo Ibsen L. Assessment of foundation design for offshore monopiles unprotected against scour. Ocean Eng May 2013;63:17–25.

[21] Damgaard M, Ibsen LB, V Andersen L, Andersen JKF. Cross-wind modal properties of offshore wind turbines identified by full scale testing 2013;116:94–108.
[22] Camp TR, Morris MJ, van Rooij R, van der Temple J, Zaaijer M, Henderson A, et al. Design methods for offshore wind turbines at exposed sites. Final report of the OWTES project. EU Joule III project JOR3-CT95-0284," Bristol United Kingdom. 2004.
[23] Hydrodynamic loading on offshore wind turbines. In: Henderson AR, editor. Design methods for offshore wind turbines at exposed sites. Delft, Netherlands: Delft University of Technology; 2003. Section Wind Energy.
[24] Adhikari S, Bhattacharya S. Dynamic analysis of wind turbine towers on flexible foundations. J Shock Vib 2012;19:37–56.
[25] Carter JMF. North Hoyle offshore wind farm: design and build. Proc ICE- Energy 2007:21–9.
[26] ASTM E647. Standard test method for measurement of fatigue crack growth rates. 2008.
[27] BS EN ISO 11782–2. Corrosion of metals and alloys- Corrosion propagation testing using precracked specimens. 2008.
[28] Deans WF, Richards CE. A technique for measuring crack length and load in compact fracture mechanics using strain gauges. J Test Eval 1979;7(3).
[29] Riddell T, Piascik S. A back face strain compliance expression for the compact tension specimen. NASA TM-208453," Hampton, Virginia. 1998.
[30] Huh Y, Song J-H. Back face strain compliance calibration for the four-point bend specimen. KSME Int J 2000;14(3):314–9.
[31] Newman JC, Yamada Y, James MA. Back-face strain compliance relation for compact specimens for wide range in crack lengths. Eng Fract Mech Oct. 2011;78(15):2707–11.
[32] ASTM D1141. Standard practice for the preparation of subtitute ocean water. 2008.
[33] Shaw WJD, Zhao W. Back face strain calibration for crack length measurements. J Test Eval 1994;22:512–6.
[34] Scott PM, Silvester DRV. The influence of seawater on fatigue crack propagation in structural steels, in United Kingdom offshore steel research project. 1975.
[35] Scott PM, Silvester DRV. The influence of mean tensile stress on corrosion fatigue crack growth in structural steels immersed in seawater, in United Kingdom offshore steel research project. 1977.
[36] Musuva JK, Radon JC. Threshold of fatigue crack growth in a low alloy steel, in Advances in fracture research. Oxford: Pergamon Press; 1982. p. 1365–72.
[37] Congleton J, Craig IH. Corrosion fatigue. In: Parkins RN, editor. In corrosion processes. Applied Science Publishers; 1982.
[38] Healy J, Billingham J. A review of the corrosion fatigue behaviour of structural steels in the strength range 350-900MPa and associated high strength weldments. Health and Safety Executive-Offshore Technology Report (OTH 532), Norwich, United Kingdom. 1997.
[39] Fukuda T, Iwadate T, Shimazaki M. Consideration on the scatter of COD and fatigue crack propagation characteristics of heavy section C-Mn-V forged steel for offshore structure. In: Offshore technology conference; 1982. p. 109–12.
[40] Bertini L. Influence of seawater and residual stresses on fatigue crack growth in C-Mn steel weld joints. Theor Appl Fract Mech Nov. 1991;16(2):135–44.
[41] Zhang W, Brook R. The effect of loading sequence on fatigue crack growth of an offshore structural steel. June. International offshore and polar engineering conference, vol. 2; 1993. p. 98–103.
[42] Vosikovsky O. Effects of stress ratio on fatigue crack growth rates in X70 pipeline steel in air and saltwater. J Test Eval 1980;8(2):68–73.
[43] Vosikovsky O. Fatigue crack growth in an X-65 pipeline steel at low cyclic frequencies in aqueous environments. Trans ASME J Eng Mater Technol 1975;97(4):294–304.
[44] Vosikovsky O. Frequency, stress ratio and potential effects on fatigue crack growth of HY 130 steel in salt water. J Test Eval 1978;6(3):175–82.
[45] Coudert E, Renaudin C. "Variable amplitude corrosion fatigue behaviour and hydrogen embrittlement of high strength steels for offshore applications. In: International offshore and polar engineering conferenceIV; 1998. p. 116–22.
[46] BS 7910. Guide to methods for assessing the acceptability of flaws in metallic structures. 2013.